



# Nano-scaled silver vanadates loaded on mesoporous silica: Characterization and photocatalytic activity

Guan-Ting Pan<sup>a</sup>, Chao-Ming Huang<sup>b</sup>, Po-Yang Peng<sup>a</sup>, Thomas C.-K. Yang<sup>a,\*</sup>

<sup>a</sup> Department of Chemical Engineering and Biotechnology, National Taipei University of Technology, Taipei, Taiwan

<sup>b</sup> Department of Environmental Engineering, Kun Shan University, Tainan, Taiwan

## ARTICLE INFO

### Article history:

Received 1 July 2010

Received in revised form

11 December 2010

Accepted 15 December 2010

Available online 15 January 2011

### Keywords:

Visible-light active photocatalyst

Mesoporous silica

Benzene

## ABSTRACT

Visible-light active silver vanadates (SVOs) loaded on mesoporous silica (SBA-15) were synthesized using a wetness impregnation procedure. All the SVO/SBA-15 composites inherit the higher photocatalytic activities and larger mineralization yields than those of P-25 (commercial TiO<sub>2</sub>) and plain SVO. Moreover, the sample loaded with 51% of SVO (51SVO/SBA-15) exhibits the best photocatalytic activity. Morphology results show that the addition of mesoporous SBA-15 favors the formation of nano-scaled silver vanadates. Surface characterization by the diffuse reflectance infrared Fourier transform spectroscopy (DRIFTS) confirms that the presence of surface hydroxyl groups on SVO/SBA-15 composites is beneficial to the adsorption kinetics. Accompanied with the results of photoluminescence spectra, the hydroxyl groups also serve as the hole-trapping centers that effectively inhibit the electron–hole recombination rate on the SVO/SBA-15 composites. Both high density of surface hydroxyl groups and low recombination rate of photogenerated charges are considered as the main factors that causes the outstanding photocatalytic activity of SVO/SBA-15 composites.

© 2010 Elsevier B.V. All rights reserved.

## 1. Introduction

Since the discovery of mesoporous silicas such as MCM-41 and SBA-15 in 1990s, there has been impressive progress in the development of highly dispersed titania–silica mesoporous composites [1–3]. The mesoporous materials typically have unique properties such as high surface area, adjustable pore size, ordered frameworks, and long-term stability which offer promising applications in adsorption, separation, and catalysis. However, the use of TiO<sub>2</sub>/SBA-15 material as a highly efficient visible-light active photocatalyst was still hindered by two shortcomings. First, titanium dioxide suffers from low efficiency under visible light illumination since it has the large band-gap energy of 3.2 eV. Second, the most general method for synthesizing titanium dioxide semiconductors involves the thermal hydrolysis or sol–gel method. These preparation schemes require the higher temperature calcinations (400 °C or higher) for better crystallinity. In recent years, Ag<sub>2</sub>ZnGeO<sub>4</sub> [4], Ag<sub>3</sub>VO<sub>4</sub> [5], and BiVO<sub>4</sub> [6] were found to be effective as the visible-light active photocatalysts for water splitting and pollutant decomposing under visible-light illumination. These photocatalysts were prepared by hydrothermal synthesis method since

this method offers many advantages, such as controllable particle size, high degree of crystallinity, and high purity while using milder synthesis temperatures and simpler process configurations.

In the present work, we demonstrated the preparation of silver vanadates–silica composites through hydrothermal synthesis using a post-synthesis step, without high-temperature calcinations. Photodecomposition of benzene was selected as a model reaction to evaluate the photocatalytic performance of silver vanadates–silica composites since benzene is a common atmospheric indoor and industrial air pollutant. The formation of intermediates during photodegradation maybe genotoxic and carcinogenic [7–9]. Therefore, the development of photocatalysts that can minimize intermediates during photocatalytic process is also formation of urgently demanded.

## 2. Experimental

### 2.1. Preparation of photocatalyst

SBA-15, a silica substrate, was synthesized with Pluronic P123 (EO<sub>20</sub>PO<sub>70</sub>EO<sub>20</sub>, M<sub>av</sub> = 5800; Aldrich) and tetraethylorthosilicate (TEOS) according to the previous report [10]. Briefly, 4.0 g of P123 was dissolved in 30 g of de-ionized water and 120.0 g of HCl solution (2 M) with stirring at 40 °C for 2 h with complete mixing. Then 8.5 g of TEOS into the P123 solution for another 22 h until a white gel was precipitated. The gel was transferred to a Teflon bottle and

\* Corresponding author at: No. 1, Sec. 3, Chung-hsiao E. Rd., Taipei 106, Taiwan ROC. Tel.: +886 2 2771 4193 2533; fax: +886 2 27760985.

E-mail address: [ckyang@ntut.edu.tw](mailto:ckyang@ntut.edu.tw) (T.C.-K. Yang).

heated at 100 °C for 24 h. The precipitate was filtered, washed several times with de-ionized water, dried overnight at 80 °C, and then calcined at 500 °C (heating rate of 1 °C/min) for 4 h in air.

The silver vanadates-loaded SBA-15 was prepared by the wetness impregnation technique. In a preparation process, 0.204 g AgNO<sub>3</sub> was dissolved in the urea aqueous solution (120 g H<sub>2</sub>O, 0.577 g urea) with stirring at room temperature for 0.5 h to obtain the solution A. Meanwhile, the mixture solution B was prepared by mixing 0.047 g NH<sub>4</sub>VO<sub>3</sub> together with 0.3 g SBA-15 in de-ionized water at 70 °C for 1 h under ultrasonic bath. Then, a suspension was formed while the solution A was added dropwise to the mixture B under vigorous stirring for 1 h. The molar composition of the suspension AgNO<sub>3</sub>/NH<sub>4</sub>VO<sub>3</sub>/CO(NH<sub>2</sub>)<sub>2</sub> was 3.0/1.0/12.0. The suspension was titrated to pH 7 using ammonia solution, followed by additional stirring at room temperature for 24 h. Finally, the as-obtained suspension was transferred into a Teflon liner autoclave with the hydrothermal treatments (temperature: 140 °C, time: 4 h). After hydrothermal procedure, the resulting precipitates were collected and washed repeatedly with de-ionized water three times, and then dried at 80 °C for 12 h. The percentage of silver vanadates was 17%, 34%, and 51% the weight ratio of  $W_{\text{SVO}}/(W_{\text{SVO}} + W_{\text{SBA-15}})$ . These samples were noted as *x*SVO/SBA-15, where *x* represents the weight percentage of silver vanadates loaded (wt%). The sample synthesized with the same condition without the addition of SBA-15 was denoted as SVO.

## 2.2. Sample characterization

The X-ray diffraction (XRD) patterns of the powders were measured using an X-ray diffractometer (PANalytical X'Pert PRO) with Cu radiation ( $\lambda = 0.15418$  nm) in the  $2\theta$  range from 20° to 60°. Transmission electron microscope (TEM) images of the composites were carried out using a field emission gun transmission microscope (Philip Tecnai G2 F20) at an acceleration voltage of 200 kV. Photoluminescence (PL) spectra were recorded by a fluorescence spectrophotometer (Dongwoo Optron) under the excitation light at 325 nm. In situ DRIFTS measurements were performed using a PerkinElmer FTIR spectrometer (spectrum GX) and a diffuse reflectance accessory (Harrick Scientific, DRP-PE9) with a temperature and atmospheric controlled high temperature and low pressure reaction cell (Harrick Scientific, HVC-DRP-3). Prior to the IR measurements, the samples were dehydrated under vacuum from room temperature to 250 °C at 10 °C/min in N<sub>2</sub> flow (30 ml min<sup>-1</sup>), held at 250 °C for 30 min, and then cooled to 30 °C. DRIFT spectra with a resolution of 4 cm<sup>-1</sup> were collected in the interval of 2800–4000 cm<sup>-1</sup> for surface hydroxyl functional groups and in the interval of 1000–2000 cm<sup>-1</sup> for surface acidity, respectively. UV–vis spectra were collected by a spectrophotometer (JASCO V-500) equipped with an integrated sphere assembly over the range of 400–700 nm. The surface area and pore volume of the as-prepared samples were determined using a volumetric sorption analyzer (Micromeritics ASAP 2020). The samples were degassed at 200 °C in vacuum condition for a period of at least 4 h prior to measurements. The nitrogen adsorption/desorption isotherms were measured over a relative pressure ( $P/P_0$ ) range from approximately 10<sup>-3</sup> to 0.995. The surface areas were calculated by Brunauer–Emmett–Teller (BET) equation using adsorption data in  $P/P_0$  ranging from 0.06 to 0.2. The pore size distributions were determined from the analysis of the adsorption isotherm, using the Barret–Joyner–Halenda (BJH) algorithm. The total pore volumes were estimated from the adsorbed N<sub>2</sub> amount at  $P/P_0 = 0.973$ .

## 2.3. Photocatalytic activity evaluation with mass spectrometry

Photocatalytic activities of the samples were determined using the photodegradation of benzene under visible-light irradiation in

a photoreactor. P-25 (TiO<sub>2</sub>, Degussa Co, Germany) was used as the reference for this experiment and SVO/SBA-15 were taken accordingly for the same photocatalyst loading. The photocatalyst powder was evenly dispersed in a thin film on an annular crystal tube [11]. Prior to the experiments, the sample was pre-treated at 150 °C for 30 min in dry N<sub>2</sub> (flowing at 100 ml min<sup>-1</sup>), and the cooled to 30 °C, before the exposure to O<sub>2</sub> flow (30 ml min<sup>-1</sup>) for 60 min. Then, the inlet valve was closed and an appropriate amount of liquid benzene was injected into the reactor, producing the gaseous benzene with the concentration of 483 ppm. The photocatalytic reaction was carried out using a white daylight lamp (TOA, FL10D-EX) after the samples reached gas–solid adsorption equilibrium. The main emission band of the fluorescent lamp is occurred at 545 nm and the photon flux was measured as  $3.98 \times 10^{-7}$  Einsein/s L. To further verify the gaseous products (intermediates), the samples were monitored on-line with a quadrupole mass spectrometer (SRS QMS300) at a regular interval.

## 3. Results and discussion

### 3.1. X-ray diffraction analysis

The XRD patterns of SBA-15 with SVO/SBA-15 and SVO with SVO/SBA-15 were shown in Fig. 1. Fig. 1a showed the low angle XRD patterns of SBA-15 and SVO/SBA-15 samples. The XRD pattern of SBA-15 shows three well resolved peaks with a sharp one at 0.98° and two weak peaks near 1.5° and 2.0° corresponding to (1 0 0), (1 1 0), and (2 0 0) reflections of an ordered hexagonal *p6mm* space group. For SVO/SBA-15 samples, the XRD peaks reduced in intensity, indicating the incoherent character of X-rays scattered by a disordered distribution of SVO particles inserted within the mesoporous channels. For the samples with the high SVO content, the intensities of the peaks are much weaker but still can be discerned, demonstrating the uniform porous structure of SBA-15 is retained.

Fig. 1b shows wide angle XRD patterns of SVO and three SVO/SBA-15 samples. As can be seen, the SVO/SBA-15 composites have two kinds of XRD patterns, assigned to the pure  $\alpha$ -Ag<sub>3</sub>VO<sub>4</sub> (JCPDS 43-0542), for 17SVO/SBA-15 and 34SVO/SBA-15 samples and to the mixed phases of Ag<sub>4</sub>V<sub>2</sub>O<sub>7</sub> (JCPDS 77-0097) and  $\alpha$ -Ag<sub>3</sub>VO<sub>4</sub> for 51SVO/SBA-15, respectively. The bulk SVO had the same crystalline structure with 51SVO/SBA-15. Based on the Scherrer's equation, the corresponding crystal sizes of SVO, 17SVO/SBA-15, 34SVO/SBA-15, and 51SVO/SBA-15 were estimated to be 58, 12, 13, and 15 nm. As the loading amount of silver vanadates increases over SBA-15, the crystal sizes of silver vanadates slightly increase.

### 3.2. Porosity and surface area characterization

The N<sub>2</sub> adsorption–desorption isotherms of SBA-15 show type IV adsorption with a H1 hysteresis loop belonging to mesoporous characteristic. With regarding to a larger hysteresis loop occurs after  $P/P_0 = 0.60$  adsorption–desorption isotherm of SVO/SBA-15, indicating that SVO/SBA-15 has more mesopores and broader pore size distribution. Moreover, an increase of the pore diameter in the mesopore range was found in SVO/SBA-15 by the inflection point of  $P/P_0$  position (Fig. 2). It is noticeable that the specific surface area and pore volumes of SVO/SBA-15 samples significantly decrease with the increase of silver vanadates loading except the pore diameters (Table 1). When the SVO/SBA-15 composites were synthesized using a post-synthesis step, the silver and vanadate species reacted on the surface of the SBA-15. As a consequence, the increasing the amount of the silver and vanadate species results in the decreases in the surface area and pore volume of the SVO/SBA-15 composites. The average pore diameters of the composites are wider than that

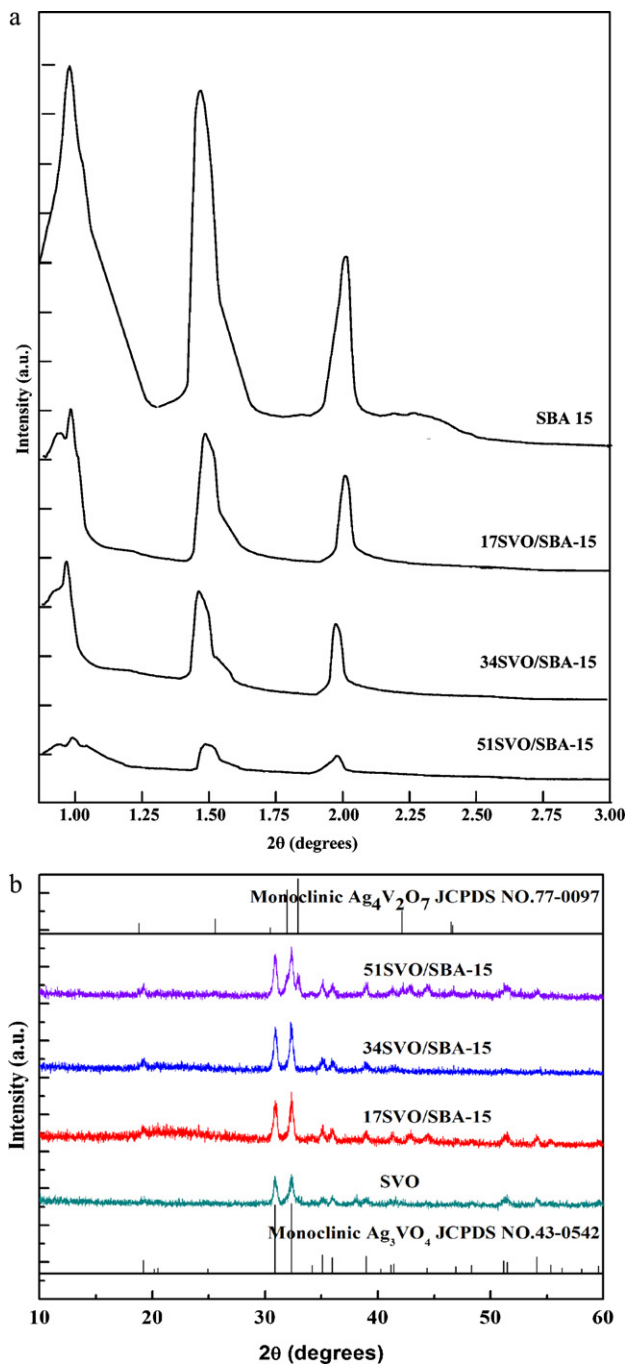


**Fig. 1.** (a) Low angle XRD patterns of SVO and SVO/SBA-15; (b) wide angle XRD patterns of SVO and SVO/SBA-15.

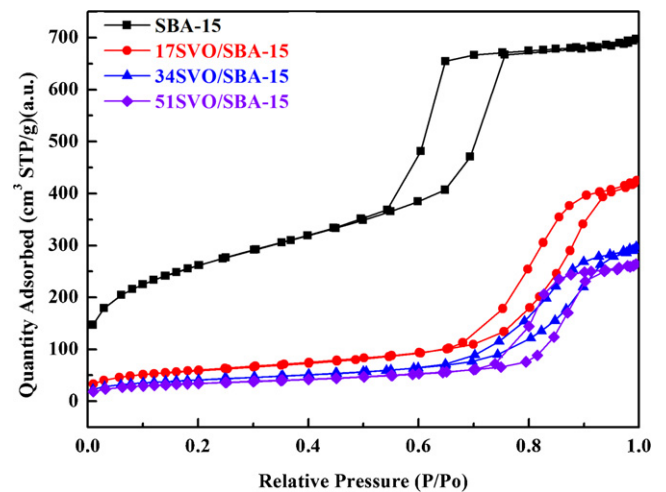


**Fig. 2.** N<sub>2</sub> adsorption–desorption isotherms of SBA-15 and SVO/SBA-15 samples.

of SBA-15, because some small pores were covered by nano-sized silver vanadate nanoparticles.

### 3.3. Characterization

To obtain further information about the formation of SVO nanocrystals on the mesopores and explore the effect of SVO on the pore structure of SVO/SBA-15 photocatalyst, HRTEM images were recorded. HRTEM images of SBA-15 and SVO/SBA-15 samples are shown in Fig. 3. The highly ordered mesoporous channel structure of pure SBA-15 is observed in Fig. 3a. A center-to-center distance is around 13 nm and a pore diameter is estimated around 7 nm, in agreement with N<sub>2</sub> adsorption–desorption results. When SVO was added in relative low amount, SVO species are well dispersed in the channel of SBA-15 and the regular silica structure is maintained in the case of 17SVO/SBA-15. As the SVO loading increases to 51 wt% (Fig. 3b), the introduction of SVO does not destroy the ordered array of mesopores and the less white channels mean more occupation. The morphology results indicate that nanocrystalline SVO was inserted the mesoporous channels of the SBA-15 when using urea as the chelating agent which exhibits a strong interaction between urea and metal ions and prevents the precipitation of silver and vanadium ions before the formation of silver vanadates–silica composites. EDX elemental analysis of a selected point of the SBA-15 and the SBA-15 supported catalyst (Fig. 3) confirms the presence of SVO particles in the center of a SBA-15 channel (normalized zirconium concentrations in parentheses).

### 3.4. Effect of SVO loading on the photodegradation activity of SVO/SAB15 composite

To further investigate the role of support (i.e., beneficial or detrimental effect) during the photocatalytic degradation, photocatalytic reactions are based on bare SVO. Since only the

**Table 1**  
Specific surface area, pore properties, and hydroxyl functional group of SBA-15, SVO/SBA-15, P25, and SVO materials.

Sample	S <sub>BET</sub> (m <sup>2</sup> g <sup>-1</sup> )	Pore volume (cm <sup>3</sup> g <sup>-1</sup> )	Pore size (nm)	Hydroxyl functional group (OH)
SBA-15	942	1.04	6.3	–
17SVO/SBA-15	217	0.66	11.9	1445.1
34SVO/SBA-15	149	0.46	12.3	1810.4
51SVO/SBA-15	125	0.41	13.3	2666.7
P25	56	0.25	17.5	10.9
SVO	2.04	0.002	7.3	836.8

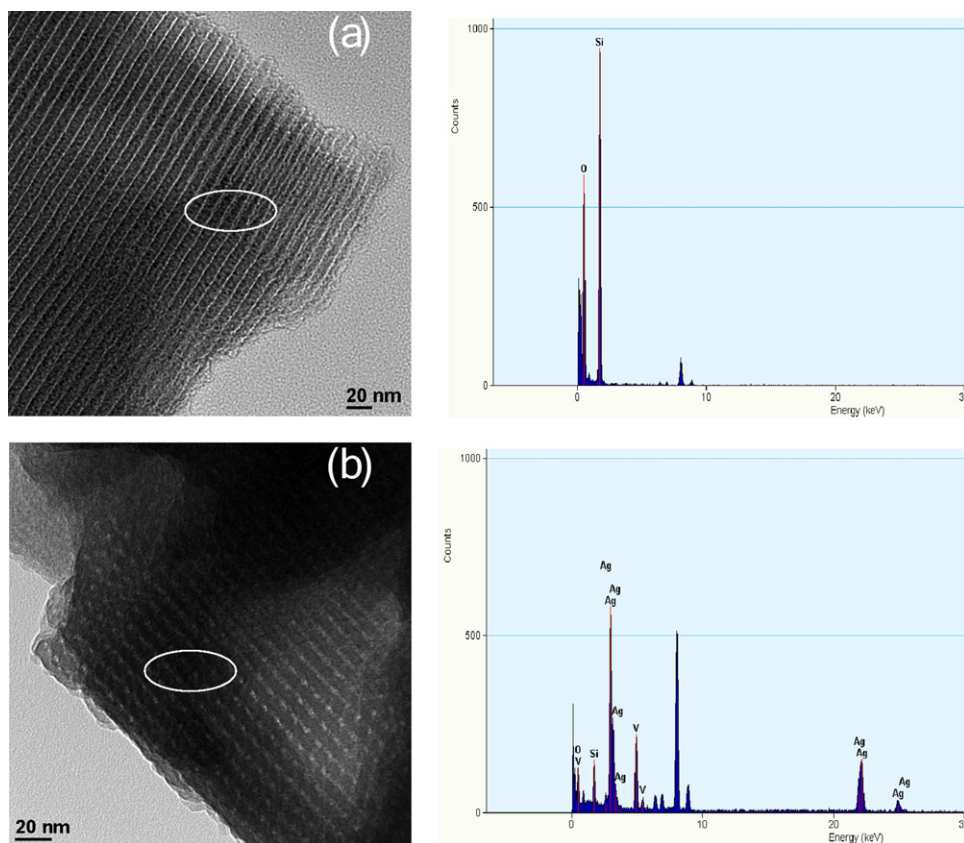


Fig. 3. HRTEM images of samples: (a) SBA-15 and (b) 51SVO/SBA-15.

semiconductor particles exhibit photocatalytic activity, the amount of composites taken to evaluate is determined according to the same active SVO content. Therefore, 0.05 g of SVO, 0.29 g of 17SVO/SBA-15, 0.15 g of 34SVO/SAB-15, and 0.10 g of 51SVO/SAB-15 were used, respectively. During the photodegradation reactions, there are two factors leading to the decreasing of the concentration of pollutant: the adsorption capacity and photocatalytic activity of photocatalyst. Table 2 indicates the adsorption capacity and photocatalytic performance of various samples. The adsorption capacity is evaluated by the adsorption amount per the surface area of the sample, which is obtained from the adsorption amount divided by actual specific surface area of the sample, as indicated in Table 2. In the absence of irradiation, the composite samples exhibit a much lower adsorption capability of gaseous benzene than that of plain SVO. At 17SVO/SBA-15 sample, the adsorption capacity is as low as 0.0029 mg. When the silver vanadate content increases to 34% (34SVO/SBA-15), the adsorption capacity increases to 0.0087 mg, which is three times higher than previous one. Increasing the silver vanadate content to 51%, the adsorption capacity increases to 0.0167 mg. Obviously, the benzene adsorption capacity is greatly

influenced by the silver vanadate content of SVO/SBA-15 composites.

As shown in Table 2, all the SVO/SBA-15 samples give the higher apparent rate constants than that of the bulk SVO. To investigate the effectiveness of the catalyst, the reaction was carried out for 12 h and the mineralization yields were reported in Table 2. Only 6% benzene was mineralized to carbon dioxide in the presence of Degussa P-25 and 29% for SVO. However, nearly 70% of mineralization yield was obtained in the presence of 51SVO/SBA-15 and about 50% mineralization yields were observed in case of 17 and 34SVO/SBA-15. Apparently, all the supported catalysts give superior photocatalytic activities than those of P-25 and SVO. Regarding SVO/SBA-15 composites, the mesoporous support helps to synthesize SVO nanoparticles. As shown in HRTEM, the presence of more active sites near the adsorbed benzene molecules results in faster degradation rates. In this study, the photocatalytic activity of composite samples was decreased in the order of 51SVO/SBA-15 > 34SVO/SBA-15 > 17SVO/SBA-15. Generally speaking, the photocatalytic activity is strongly related to the crystalline phase. Konta et al. [12] reported that  $\alpha$ -Ag<sub>3</sub>VO<sub>4</sub> has stronger

Table 2

Adsorption capacity, apparent rate constant, and mineralization performance of P25, SVO, and SVO/SBA-15 under 720 min of irradiation.

Sample	Adsorption amount (mg)	Adsorption amount per surface area (mg/m <sup>2</sup> ) <sup>a</sup>	Apparent rate constant (min <sup>-1</sup> )	Mineralization yield (%)
17SVO/SBA-15	0.1799	0.0029	0.1799	62.93
34SVO/SBA-15	0.1949	0.0087	0.1949	22.35
51SVO/SBA-15	0.2091	0.0167	0.2091	12.50
P25	0.0380	0.0136	0.0380	2.80
SVO	0.0563	0.5520	0.0563	0.10
SBA-15	0.0047	0.0000	–	–

<sup>a</sup> Adsorption amount per the surface area = adsorption amount/actual surface; actual surface area = sample weight × specific surface area.

**Table 3**Adsorptions of benzene (peak at 1484 cm<sup>-1</sup>) and phenol (peak at 1604 cm<sup>-1</sup>) on various samples after 3 and 5 min of illumination.

Sample	Irradiation for 0 min		Irradiation for 3 min		Irradiation for 5 min	
	Benzene	Phenol	Benzene	Phenol	Benzene	Phenol
P25	683.6	0	642.5	820.1	522.7	648.9
SVO	5154.2	0	4154.2	4568.4	2235.7	527.5
17SVO/SBA-15	9904.7	0	7523.8	5398.2	1.3	4.2
34SVO/SBA-15	12,493.0	0	8473.1	8038.9	0.1	0.3
51SVO/SBA-15	14,933.9	0	9178.7	10,855.8	0.0	0.0

photocatalytic activity than those of  $\beta$ -AgVO<sub>3</sub> and Ag<sub>4</sub>V<sub>2</sub>O<sub>7</sub> for oxygen-production from water-splitting under visible-light irradiation. In this study, it was observed that the 51SVO/SBA-15 sample, with mixed phases of Ag<sub>4</sub>V<sub>2</sub>O<sub>7</sub> and  $\alpha$ -Ag<sub>3</sub>VO<sub>4</sub>, exhibits the highest photocatalytic activity, compared to that of 34SVO/SBA-15 with only one high crystallinity  $\alpha$ -Ag<sub>3</sub>VO<sub>4</sub> phase. This implies that a bicrystalline framework of crystalline structure show much better photocatalytic activity than that of single phase [11,13–15].

### 3.5. Role of surface hydroxyl groups on the degradation of benzene

From Tables 1 and 2, the adsorption of gaseous benzene is highly relevant to the contents of silver vanadate in SVO/SBA-15 composites due to the stronger affinity between benzene and the sample surface. Furthermore, the surface OH functional group on photocatalyst has been found to provide the adsorption centers for reagents and/or products. At the meantime, they are also considered as the precursors of hydroxyl radicals responsible for oxidation reactions [16,17]. To quantify the intensity of the OH group on

the samples, in situ DRIFTS experiments were conducted. Before DRIFTS measurements, the samples were dehydrated at 250 °C. Two broad strong bands, ranging from 3700 to 3100 cm<sup>-1</sup>, were observed for SVO [11]. A deconvolution procedure was applied to calculate the amounts of various OH groups. The amount of OH groups was decreased in the order of 51SVO/SBA-15 > 34SVO/SBA-15 > 17SVO/SBA-15 > SVO > P25 as shown in Table 1. To further verify the effect of surface hydroxyl groups on the adsorption of benzene molecules, benzene interaction with the surfaces of the samples, under darkness and visible-light illumination, was also studied using in situ DRIFTS. In the case of benzene adsorption, some significant bands including the  $\nu_4$  parallel band at 684 cm<sup>-1</sup> and three perpendicular bands  $\nu_{12}$  at 3048 cm<sup>-1</sup>,  $\nu_{13}$  at 1484 cm<sup>-1</sup>,  $\nu_{14}$  at 1038 cm<sup>-1</sup>, and a few combination bands were observed [18]. The C–H bending band of benzene (1484 cm<sup>-1</sup>) was selected to represent the benzene molecules adsorbed on the samples (Fig. 4). Comparing in Fig. 4a, b, and c the sample 51SVO/SBA-15 has the maximum adsorption and fast photocatalytic rate without the formation of intermediate (phenol) during 5 min illumination. The quantitative results were also summarized in Table 3. From Table 3,

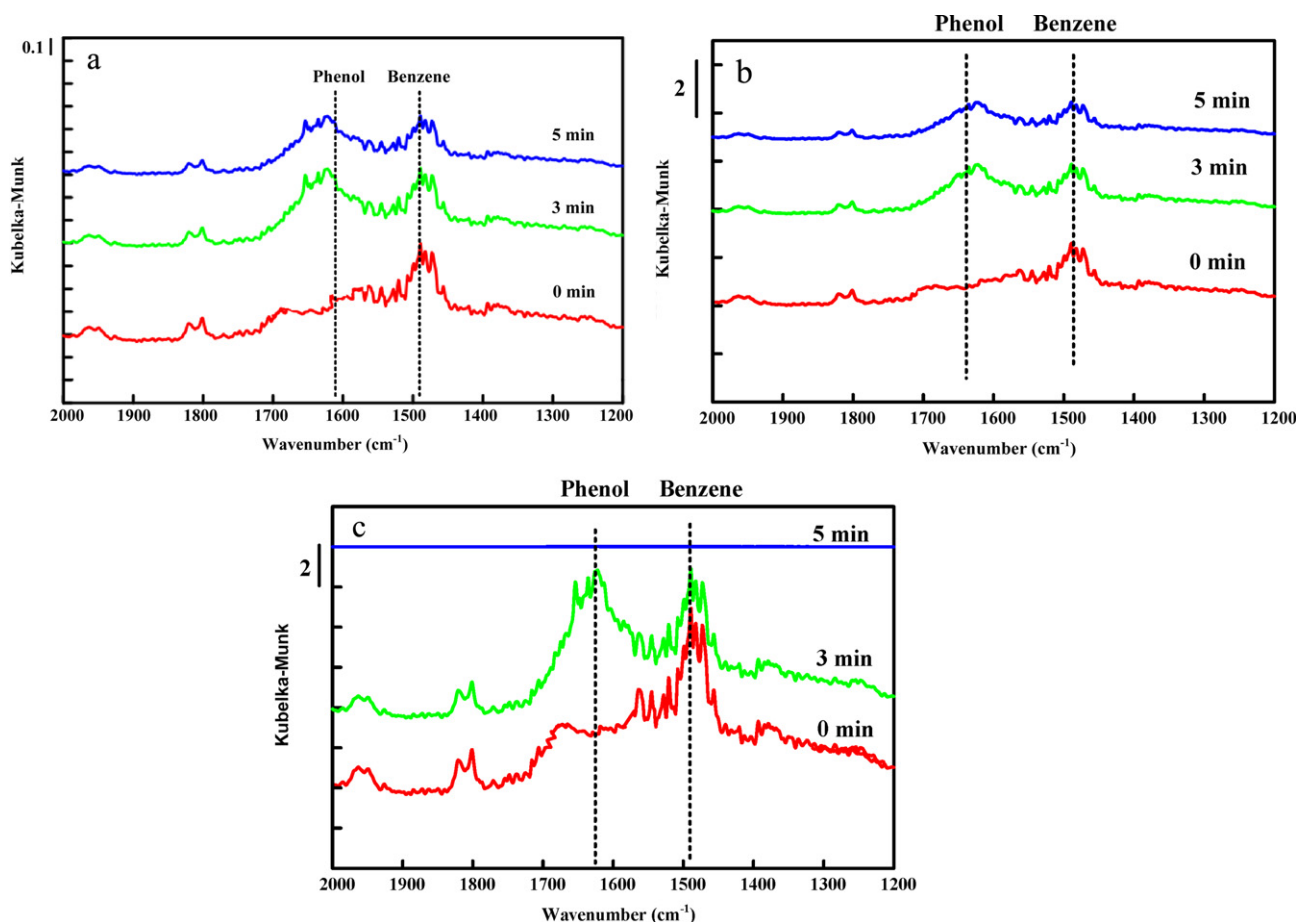


**Fig. 4.** Time-dependent DRIFT spectra of adsorbed benzene and phenol on various samples during the visible-light irradiation: (a) P25, (b) SVO, and (c) 51SVO/SBA-15.

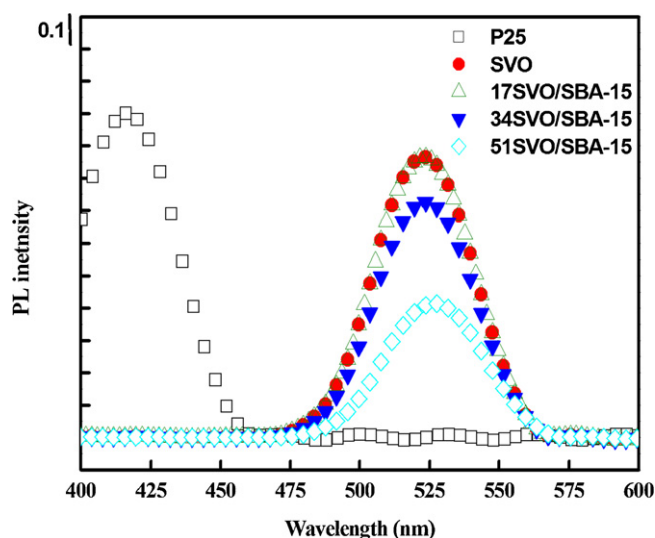


Fig. 5. Normalized PL intensity of the samples measured at 300 K.

the adsorption capacity of benzene on the composite samples, strongly related to the intensity of OH groups, played a rate-determining step in the photocatalytic reaction. The intermediates found in the gas phase or on the surface of catalyst were recognized as in the secondary pollution, in some cases, which are more toxic than their parent compounds [19,20,21]. As shown in Fig. 4, the peak at  $1604\text{ cm}^{-1}$  attributed to the ring stretching of phenol was observed and phenol was the only quantifiable intermediate detected in this study. The quantitative results of phenol in the dark for 30 min and after 3 and 5 min of illumination are also listed in Table 3. The amount of adsorbed phenol on the loaded sample is much higher than those of P25 and SVO during the 3 min illumination. As the irradiation time increases to 5 min; the adsorbed phenol on the SVO/SBA-15 compounds became negligible as shown in Fig. 4. Nearly 100% of benzene was degraded on the surface of composite materials. However, sensible amount of phenol were observed in the case of P25. Apparently, an enhanced mineralization yield was achieved using SVO/SBA-15 composites. The superior photocatalytic activity of SVO/SBA-15 composites may be due to the existence of abundant surface hydroxyl groups. OH groups were considered as strong Brønsted acid sites which provide more surface adsorption centers for reactants. These groups inherited extraordinarily reactive hydroxyl group radicals, which are capable to oxidize the adsorbed substrates. As a result, the accelerating ion of the photocatalytic process was achieved [22–24]. Moreover, the highly polarized state of strong Brønsted acid sites also serve as effective hole-trapping centers, thus limiting undesirable photo-carrier recombination. Thus, it can be concluded that nano-scaled  $\alpha\text{-Ag}_3\text{VO}_4$  crystals with abundant surface hydroxyl groups are proved to be a crucial factor in the enhancement of photocatalytic activity.

### 3.6. Photoluminescence spectra

Photoluminescence (PL) spectra have been widely used to disclose the migration, transfer, and recombination processes of the photogenerated electron–hole pairs in the semiconductor particles [25]. Fig. 5 shows the PL spectra normalized with the photoabsorption intensity for P25, SVO, and SVO loaded composites at room temperature. The normalized PL intensity of these samples decreases in the order of  $\text{P25} > \text{SVO} > 17\text{ SVO/SBA-15} > 34\text{SVO/SBA-15} > 51\text{SVO/SBA-15}$ . The PL of SVO/SBA-15 samples show obvious decrease as compared to that of SVO, indicating the recombina-

tion of photoelectrons and holes is efficiently suppressed in the composite semiconductors. The intensity of normalized PL spectra corresponds to the recombination rates of the holes formed in the  $\text{O}_{2p}$  band and the electron in the  $\text{V}_{3d}$  band. The slower recombination process of photogenerated charges (the less the PL intensity) can facilitate the enhancement of photocatalytic activity of SVO/SBA-15 composite.

## 4. Conclusions

Nanocrystalline SVO/SBA-15 materials were synthesized using a post-synthesis process.  $\text{N}_2$  adsorption–desorption isotherms confirm that the mesoporous structure of SBA-15 is maintained. XRD and HRTEM results indicate the nano-sized  $\alpha\text{-Ag}_3\text{VO}_4$  for 17 and 34SVO/SBA-15 and to the mixed phases of  $\text{Ag}_4\text{V}_2\text{O}_7$  and  $\alpha\text{-Ag}_3\text{VO}_4$  for 51SVO/SBA-15 are dispersed in the channel or on the surface of SBA-15. The DRIFT spectra identify the formation of toxic intermediate, phenol, on the surface of SVO/SBA-15 composites. A high residue of phenol is observed during benzene degradation on P-25 whereas the amount of phenol is negligible in the case of SVO/SBA-15 samples. The composite photocatalyst exhibits highly enhanced photocatalytic activity under visible light irradiation, and the highest efficiency is for the 51SVO/SBA-15 composite. The enhanced activity is attributed to the abundant surface hydroxyl groups and the reduction of the recombination rate of photogenerated hole–electron pairs. The application of SVO/SBA-15 not only favors the degradation of benzene, leading to the breakage of the benzene ring, but also facilitates the quick conversion of the intermediate phenol, to final product  $\text{CO}_2$ . The composite photocatalyst is promising for air purification application for its strong adsorption and visible-light photocatalytic activity.

## Acknowledgement

This work was financially supported by the National Science Council, Taiwan, ROC, under grant NSC 99-2221-E-027-078-MY2.

## References

- [1] J. Yang, J. Zhang, L. Zhu, S. Chen, Y. Zhang, Y. Tang, Y. Zhu, Y. Li, J. Hazard. Mater. B137 (2006) 952.
- [2] D.R. Sahu, L.Y. Hong, S.C. Wang, J.L. Huang, Micropor. Mesopor. Mater. 117 (2009) 640.
- [3] W.T. Qiao, G.W. Zhou, X.T. Zhang, T.D. Li, Mater. Sci. Eng. C 29 (2009) 1498.
- [4] X. Li, S. Ouyang, N. Kikugawa, J. Ye, Appl. Catal. A: Gen. 334 (2008) 51.
- [5] C.M. Huang, G.T. Pan, Y.C.M. Li, M.H. Li, T.C.K. Yang, Appl. Catal. A: Gen. 358 (2009) 164.
- [6] C.M. Huang, G.T. Pan, P.Y. Peng, T.C.K. Yang, J. Mol. Catal. A: Chem. 327 (2010) 38.
- [7] M.O. Bachmann, J.E. Myers, Soc. Sci. Med. 40 (1995) 245.
- [8] X.Z. Fu, W. Zeltner, M.A. Anderson, Appl. Catal. B: Environ. 6 (1995) 209.
- [9] J. Zhong, J. Wang, L. Tao, M. Gong, L. Zhimin, Y. Chen, J. Hazard. Mater. B139 (2007) 323.
- [10] D. Zhao, J. Feng, Q. Huo, N. Melosh, G.H. Fredrickson, B.F. Chmelka, G.D. Stucky, Science 279 (1998) 548.
- [11] L.C. Chen, G.T. Pan, T.C.-K. Yang, T.W. Chung, C.M. Huang, J. Hazard. Mater. 178 (2010) 644.
- [12] R. Konta, H. Kato, H. Kobayoshi, A. Kudo, Phys. Chem. Chem. Phys. 5 (2003) 3061.
- [13] Z. Ding, G.Q. Lu, P.F. Greenfield, J. Phys. Chem. B 104 (2000) 4815.
- [14] G. Liu, Z. Chen, C. Dong, Y. Zhao, F. Li, G.Q. Lu, H.M. Cheng, J. Phys. Chem. B 110 (2006) 20823.
- [15] G. Liu, X. Wang, Z. Chen, H.M. Cheng, G.Q. Lu, J. Colloid Interface Sci. 329 (2009) 331.
- [16] A.J. Maira, K.L. Yeung, C.Y. Lee, P.L. Yue, C.K. Chan, J. Catal. 192 (2000) 185.
- [17] X. Wang, J.C. Yu, P. Liu, X. Wang, W. Su, X. Fu, J. Photochem. Photobiol. A: Chem. 179 (2006) 339.
- [18] G. Di Lonardo, L. Fusina, G. Masciarelli, F. Tullini, Spectrochim. Acta A 55 (1999) 1535.

- [19] G.R.M. Echavia, F. Matzusawa, N. Negishi, *Chemosphere* 76 (2009) 595.
- [20] W.A. Jacoby, D.M. Blake, J.A. Fennell, J.E. Boulter, L.M. Vargo, M.C. George, S.K. Dolberg, J. *Air Waste Manage. Assoc.* 46 (1996) 891.
- [21] S. Zhang, Z. Zheng, J. Wang, J. Chen, *Chemosphere* 65 (2006) 2282.
- [22] M. Niwa, K. Suzuki, K. Isamoto, N. Katada, *J. Phys. Chem. B* 110 (2006) 264.
- [23] K.M. Parida, M. Acharya, S.K. Samantaray, T. Mishra, *J. Colloid Interface Sci.* 217 (1999) 388.
- [24] X.C. Wang, J.C. Yu, P. Liu, X.X. Wang, W.Y. Su, X.Z. Fu, *J. Photochem. Photobiol. A* 179 (2006) 339.
- [25] H. Yamashita, Y. Ichihashi, S.G. Zhang, Y. Matsumura, Y. Souma, T. Tatsumi, M. Anpo, *Appl. Surf. Sci.* 121 (1997) 305.